Improved performance of polyimide Cirlex based dielectric barrier discharge plasma actuators for flow control

J. Nunes-Pereira[1, 2, *], F. F. Rodrigues[1], M. Abdollahzadeh[1], J.C. Páscoa[1] and S. Lanceros-Mendez[3, 4, *]

[1] C-MAST, Centre for Mechanical and Aerospace Science and Technologies, Universidade da Beira Interior, Rua Marquês d'Ávila e Bolama, 6200-001 Covilhã, Portugal

[2] CF-UM-UP, Centro de Física das Universidades do Minho e do Porto, Campus de Gualtar, 4710-057 Braga, Portugal

[3] BCMaterials, Basque Center for Materials, Applications and Nanostructures, UPV/EHU Science Park, 48940 Leioa, Spain.

[4] IKERBASQUE, Basque Foundation for Science, 48009 Bilbao, Spain

Abstract:

Dielectric barrier discharge (DBD) plasma actuators are simple electrohydrodynamic devices, which are able to provide effective aerodynamic control. One of the main components of these devices is the thin dielectric layer, which allows to separate and prevent the arc between the high voltage electrodes. Different materials can be used as dielectric layer to reduce the power consumption or boost the flow controlling effect of the actuators. In this context, this report presents a comparative study of two commercial polyimides, Kapton and Cirlex, used as dielectric layer of surface DBD plasma actuators. The electrical, dielectric, mechanical, electromechanical and thermal properties were obtained to evaluate overall performance. It was verified that Cirlex (8.3 W) consumes less power than Kapton (21.3 W) to generate higher induced flow velocity of ≈3.4 m/s for an input voltage of 11 kVpp and 24 kHz. During one AC cycle at 11 kVpp the charge transferred for Cirlex (70 nC) is lower than for Kapton (100 nC), as well as the dielectric breakdown voltage to ignite the plasma discharge, 1.5 and 2.2 kVpp, respectively. The Cirlex DBD presents a higher voltage operation limit (at least 14 kVpp) and a more regular plasma discharge, which results in a more homogenous thermal profile and temperature distribution during its operation. The Cirlex actuator delivered higher mechanical power (6.2 mW) and achieved higher electromechanical efficiency (0.004%).

The polyimide Cirlex proved to be a suitable alternative for Kapton to fabricate DBD plasma actuators for flow control with improved performance.

Keywords: Dielectric barrier discharge plasma actuators; Polyimides; Cirlex; Kapton; Flow control.

Corresponding author:
*j.nunespereira@ubi.pt (J.N.P.) and senentxu.lanceros@bcmaterials.net (S.L.M.)

1. Introduction

Active flow control is a topic of growing interest particularly in the area of fluid mechanics and aerodynamics with application in a variety of engineering systems.[1] The most obvious applications of flow control are in aviation for improving the efficiency of the aircraft, through drag and noise reduction, lift enhancement and vibration suppression. These effects will lead to optimized fuel consumption and heat transfer improvement. Flow control is typically achieved by introducing disturbances into the flow field allowing the manipulation of the original flow around a specific surface, when requested.[1,2] In this context, dielectric barrier discharge (DBD) plasma actuators appear as suitable electrohydrodynamic devices for effective aerodynamic control. Their use in flow control has gained attention due to their simple structure, low weight, low power consumption, absence of moving parts, compatibility with aerodynamic surfaces, high dynamic responses and real-time control ability.[1,3] Typically, a surface DBD plasma actuator is composed by two asymmetric electrodes (exposed and embedded), separated by an insulating dielectric material, that when subjected to a high voltage and high frequency AC signal leads to ionization of the air adjacent to the exposed electrode and to the formation of a plasma discharge. The plasma discharge beside the surface gives rise to an effective body force which pulls and pushes the ambient air.[1] This body force is also identified as induced flow velocity or ionic wind.

Several studies and application of these devices for active flow control have been reported, including numerical studies such as modelling the induced body force,[4] comparison of the flow control ability under steady and unsteady modes of actuation,[5] drag reduction on an Ahmed body via single DBD implementation at different positions,[6] flow separation control on air foils by different DBD plasma actuator models,[7] simulation

of coupled plasma and fluid flow physics of DBD,[8] 2D simulation of DBD plasma actuator for the design of an experimental setup to test the flow control on a Coanda surface,[9] among others. Further, experimental studies have been presented reporting on the implementation of DBD actuators for active flow control, such as single plasma actuator excited by two simultaneous sinusoidal voltage waveforms for both steady and unsteady modes,[10] the improvement of the stall speed on a small unmanned aerial vehicle, UAV,[11] the decrease of cross flow velocity in the boundary layer and attenuation of stationary vortex intensity by the effect of multi discharge actuation system,[12] increasing of lift coefficient and drag reduction of a delta wing by using a multi-DBD plasma actuator,[13] the drag reduction, dispersion of longitudinal vortices and suppression of the separation flow on the rear part of an Ahmed body,[14] in addition to others.

According to the literature, the most used material as dielectric layer for DBD plasma actuators fabrication is the polyimide Kapton. The processing versatility of the Kapton film together with the excellent stability of its properties over a wide range of temperature make it an excellent choice to develop the dielectric layer of DBD plasma actuator systems.[15] The material that composes the dielectric layer is essential in determining the final performance of the actuator. It must present a high dielectric strength and should be chemically and physically stable to avoid degradation in the presence of plasma. Lower dielectric constants reduce the effective capacitance of the actuator, and thus the current density, allowing higher operating voltages before the appearance of streamers in the plasma discharge and consequent saturation.[16] On the other hand, it has been shown that for a given geometry and fixed applied voltage, higher dielectric constants leads to higher induced flow velocities and higher consumed electric power.[17] A general recommendation found in the literature is that since low dielectric constants delay the saturation of plasma discharge, the use of thick dielectric layers with low dielectric constant enables improves performances of the actuators.[18]

In spite of the essential role played by the dielectric material in the performance of the DBD plasma actuators, there are few studies focussing on the search for new alternatives to the standard and most commonly used dielectrics. Polyisobutylene rubber, acetoxy silicone and polylactic acid polymers were tested in DBD plasma actuators and their performance compared to Kapton.[19] DBD based on polyisobutylene and silicone supported higher operation voltages than Kapton up to 13 kVpp, and both polyisobutylene and silicone generated higher induced flow velocities of ≈4.2 m/s for 12 kVpp and 13 kVpp, respectively. The maximum electromechanical efficiency achieved for silicone

was 0.039% higher than Kapton. The analysis of the thermal behaviour of these dielectric materials revealed that the actuators based on silicone presents the lowest temperature field with $\Delta T=12.0$ ºC, and dissipate less energy in the form of heat than the remaining ones for the same voltage range.[20] The influence of the dielectric thickness and operating frequency for Kapton, polytetrafluoroethylene (teflon) and glass reinforced epoxy resin have been also reported. The Kapton plasma actuator registered the highest induced velocity of 5.22 m/s at a frequency of 10 kHz and with a large power consumption of around 100 W.[21] The fabrication of DBD plasma actuators with different dielectric materials such as polymers, ceramics, liquid crystal polymers and composites focussing on the performance of the actuators for ozone production has been also reported .[22] The degradation of the dielectric layer is a limitation on the durability of these devices, Kapton dielectrics being reported to burn out after voltage increasing when the discharge has already entered in the filamentary regime which typically indicates that driving voltage is near the limit of the dielectric.[23] The monitoring of dielectric degradation has been conducted by measuring power consumption and capacitance changes and it has been observed that the increase of the effective capacitance of Kapton actuators is related to its degradation, leading to a subsequent increase in the power consumption.[24] Thus, polydimethylsiloxane (PDMS) coatings have been suggested to delay the onset of Kapton degradation. The simultaneous electrode aging was reported as limitation on the durability of DBD actuators, with retraction of the edges of gold electrodes followed by changes in its morphology being pointed out as reasons for the drop in the cold capacitance and the increase of effective capacitance and power consumption.[25]

Despite the excellent properties of Kapton, some of the mentioned limitations and the need of improved performance motivates the research on novel materials for dielectric layers of DBD plasma actuators. In this sense, the high-performance polyimide Cirlex appears as a promising alternative as it maintains the best properties of Kapton and broaden the application horizons with improved yields due to its thick and compact structure.[26]

This work reports a comparative study on the performance of Kapton and Cirlex based DBD plasma actuators for flow control applications. Kapton and Cirlex based plasma actuators were produced with the same geometry but in a structurally different configuration, multilayer vs. compact structure, respectively, and were characterized in terms of electric power, capacitance, dielectric breakdown, induced flow velocity, mechanical power, electromechanical efficiency and thermal characteristics. The

comparison between the properties of the DBD plasma actuators for flow control applications is presented and discussed.

2. Experimental details

2.1. Materials and DBD production

The fabrication of the DBD plasma actuators was based on the following materials: polyimide Kapton tape (Kapton HN) with 60 µm thickness, polyimide Cirlex sheet (Cirlex CL) with 1 mm thickness and two copper tape films with 10 mm width and 80 µm thickness, and 20 mm width and 80 µm thickness. To prepare the actuator based on Kapton the tape was stacked layer by layer up to a final thickness of 1 mm. The Cirlex based actuator was used as received from the supplier. The final thickness of the produced actuators was 1 mm for both materials. Copper electrodes were asymmetrically glued on either surface of both dielectrics with 1 mm gap between them. The exposed electrode has dimensions of 10 mm width, 80 mm length and 80 µm thickness (Fig. 1). The covered electrode has the same length and thickness of the previous one and 20 mm width to ensure that the extension of the plasma discharge was not limited by the end of the covered electrode.[19]

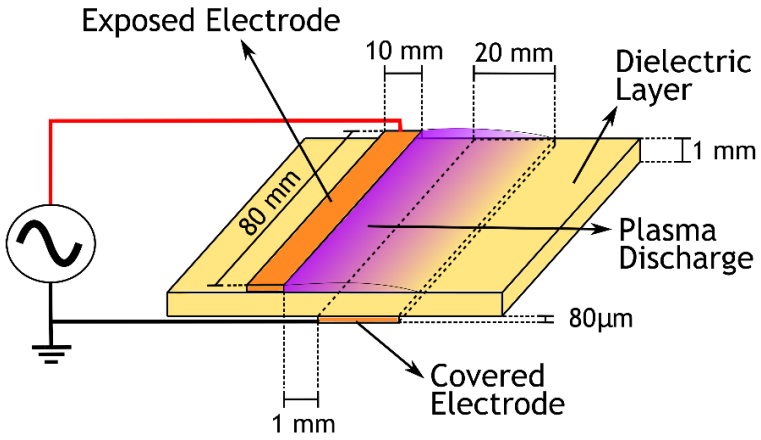


Fig. 1. Schematic representation of the DBD plasma actuators.

2.2. DBD characterization

The experimental setup depicted in Fig. 2 was used to operate and characterize the DBD plasma actuators.

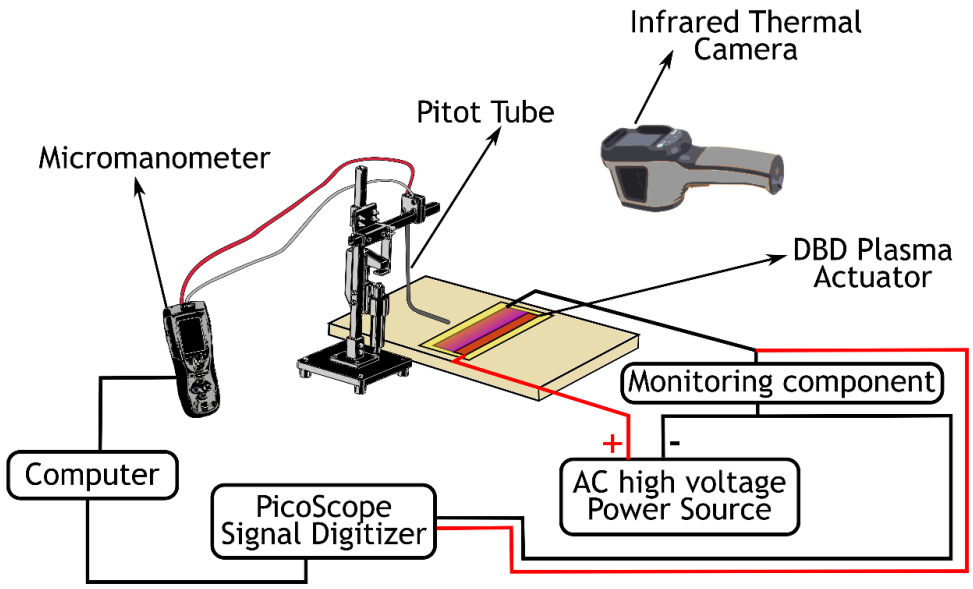


Fig. 2. Schematic representation of the experimental setup used to operate and characterize the DBD plasma actuators.

The DBD plasma actuators were powered by an AC high voltage and frequency power source (PVM 500, Information Unlimited), allowing to provide signals with voltage amplitudes up to 20 kV peak to peak (kVpp) and frequencies between 20 and 50 kHz. To perform the electrical characterization of the DBD plasma actuators, the voltage and current waveforms were registered with a digital oscilloscope (PicoScope 5443A) connected to a high voltage probe (Secondary Ignition Pickup) through two different methods that will be described below. The experimental tests were carried out at an ambient temperature of ≈22 °C and a relative humidity of 40-50%.

The electric current method was used to obtain the input current of the signal since, as high voltages were used. In the first approach, a metal resistor was placed in series with the DBD actuator so that the voltage across the resistor was low enough to be measured by a conventional probe, and the current was determined through the Ohm's law. A 100 Ω metal resistor with 1% tolerance was used, which low resistance value has no influence in actuator operation. This resistor was selected because it has a temperature coefficient of 50 ppm, which means that the impedance remains almost constant even under temperature variations, which can be neglected in the power consumption analysis.[27] The voltage and current waveforms were recorded and the average consumed power (P_{el}) of n signal periods (T) was determined by the equation (1):

$$P_{el} = \frac{1}{nT}\int_0^{nT} v(t)\,.\,i(t)dt \qquad (1)$$

where v(t) and i(t) are the input voltage and input current of the actuator, respectively. The waveforms were acquired with a sampling rate of 125 MS/s and a vertical resolution of 14 bits, which results in an uncertainty lower than 2%.

In the second approach, the electric charge method was conducted replacing the resistor by a ceramic capacitor (E222M) of 10 nF capacitance and 10% tolerance. In this method, the voltage across the actuator is reduced and the instantaneous charge (q(t)) accumulated in the capacitor was determined by the equation (2):[28]

$$q(t) = C \cdot v_c(t) \quad (2)$$

where C is the capacitance of the of the capacitor and $v_c(t)$ is the voltage across the capacitor. Plotting the instantaneous charge of the capacitor against the instantaneous voltage of the actuator results in the so-called Lissajous curves (voltage-charge cyclograms). The cyclograms allows the determination of relevant electrical parameters of the actuators such as the effective (C_{eff}) and cold (C_{cold}) capacitances through specific local slopes of the curves,[29] the breakdown voltage (V_b) and the charge transferred (dQ) for different operating input voltages.

To obtain a measure for fluid dynamic characterisation of the DBD actuators, the velocity of the induced flow was determined using a stainless-steel Pitot tube (167-6) with 1.19 and 3.18 mm inner and external diameter, respectively. The velocity profiles were measured in the middle of the exposed electrode length (spanwise direction) horizontally displaced 1.5 cm from the electrode edge (streamwise direction). This distance is assumed in the literature as where the induced flow reaches the maximum velocity.[17] The Pitot tube was mounted in a holder, removable in the vertical direction, containing an external digital micrometer, with 25 mm of maximum displacement, resolution of 0.001 and accuracy of ±0.002 mm, which allows measurements in several points along the vertical axis. The first measurement point was located 1.5 mm high from the surface of the actuator, and the subsequent measurements were vertically spaced 0.25 mm from the previous one. For each measurement, the induced velocity was acquired during 10 s at a rate of 1 sample per second and the final value presented as the average and standard deviation. The static and stagnation pressures from the Pitot tube were measured trough a differential pressure micromanometer (Extech HD 350), which automatically computes the airflow velocity with a resolution of 0.01 m/s and an accuracy of 1% FS. The micromanometer was connected to a computer allowing live streaming data.

The electromechanical behaviour of the actuators was evaluated through the mechanical power and electromechanical efficiency by a method described elsewhere.[30] This method

describes the mechanical power (P_m) delivered by the actuator to generate the flow in relation of the kinetic energy flow rate, equation (3):

$$P_m = \int_0^{\infty} \frac{1}{2} \rho u(Y)^3 l dY \quad (3)$$

where ρ is the air density, u is the velocity, Y is the vertical distance from the surface and l is the electrode length. The electromechanical efficiency (η_m) of the DBD plasma actuators can be estimated using equation (4):

$$\eta_m = \frac{P_m}{P_{el}} \times 100\% \quad (4)$$

The optical evaluation of the plasma discharge was performed using a photographic camera (OnePlus HD 1903) with a resolution of 1080 × 1920 pixels.

Finally, the thermal properties of the plasma discharge were studied by infrared thermography measurements (FLIR E50), with a resolution of 240 × 180 pixels and 2% uncertainty, on the upper surface of the DBD actuator immediately after stopping plasma discharge during 180 s of operation. Previously, the plasma actuators were painted with black matte ink with an emissivity, *e*, of 0.97. The black ink was previously validated experimentally to ensure that it did not affect the temperature fields of the actuator during operation [20].

3. Results and discussion

The voltage and current waveforms to operate the DBD plasma actuators were recorded for both electric current and current charge methods and used to compute the electric power and capacitances at different voltage levels. Fig. 3 shows representative voltage and current waveforms for Kapton and Cirlex actuators operating at 11 kVpp input voltage and 24 kHz, obtained by the electric current method. The current and voltage waveforms registered for all tested plasma actuators present similar shape and behaviour.[31,32]

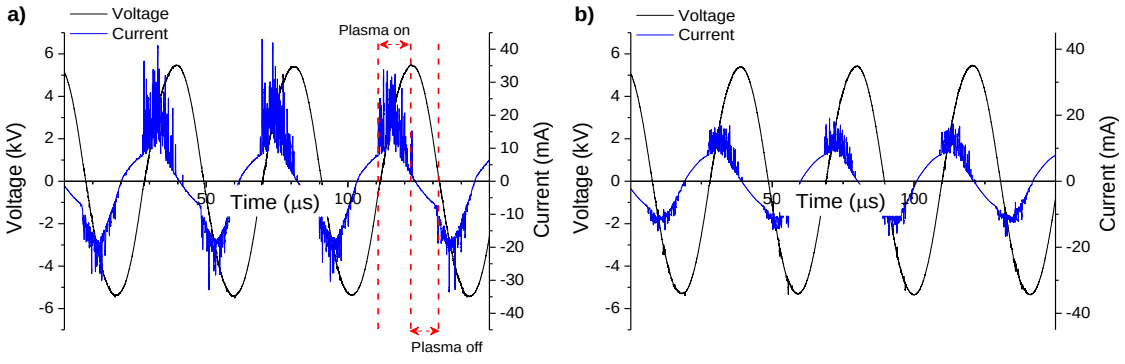


Fig. 3. Representative voltage and current waveforms for Kapton (a) and Cirlex (b) DBD plasma actuators for an input voltage of 11 kVpp at 24 kHz, obtained by the electric current method.

The discharge of a DBD plasma actuator is characterized by two microdischarge periods (plasma discharge on) alternating with two dark periods (plasma discharge off) during each AC cycle.[33] The voltage and current waveforms (Fig. 3) present sinusoidal shape, the signals being ≈90º out of phase with current leading the voltage. Further, in the current waveform are visible a series of high amplitude spikes, characteristics of AC DBD plasma actuators, as a result of fast impedance variations during each microdischarge.[31] These spikes are observed two times per each AC cycle corresponding to the moments that plasma discharge occurs. These current pulses are more intense and of greater amplitude in the positive half cycle than in the negative one, which is ascribed to the occurrence of two different plasma regimes (streamer and glow) during the AC cycle.[34,35] The streamer regime occurs during the half positive cycle and is characterized by high current pulses, whereas the glow regime takes place during the half negative cycle and presents small current pulses.[36] The Kapton (Fig. 3a) and Cirlex (Fig. 3b) voltage and current waveforms present similar behaviour, with variations just in the amplitude of the current pulses. The maximum amplitude of the current pulses for Kapton is in the order of 40 and 30 mA for the positive and negative half cycles respectively, while for Cirlex is ≈20 and 15 mA, respectively. These current pulses are directly related with the power consumption of the DBD plasma actuator as shown below.

Fig. 4 presents the electric power (P_{el}) consumed by each DBD plasma actuator as a function of the applied voltage at the frequency of 24 kHz, determined by the electric current method trough the equation (1).

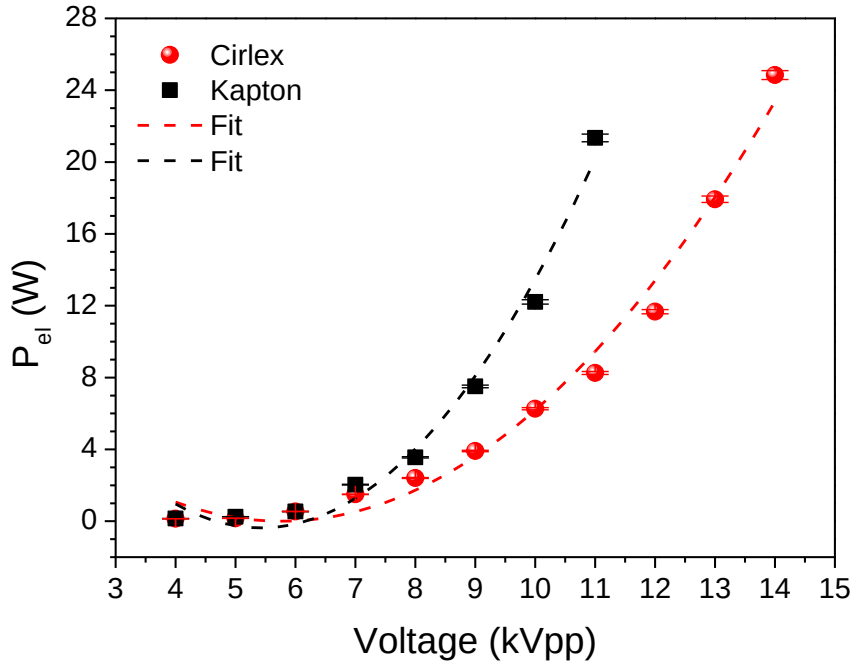


Fig. 4. Electric power consumption for Cirlex and Kapton DBD plasma actuators at 24 kHz.

The average power consumed by both DBD actuators increases with increasing input voltage, as reported for asymmetric DBD actuators in the same power range.[20,37] The electric power consumed is similar for both materials at the low voltage ranges between 4 and 6 kVpp. From 7 kVpp on, the Cirlex DBD has lower power consumption than Kapton, and this difference increases with increasing input voltage from ≈0.5 to 13 W for 7 and 11 kVpp, respectively. The operating voltage limit for Kapton is 11 kVpp, the dielectric burning-through for higher voltages, while for Cirlex it is at least 14 kVpp since the material was not tested to its limit. This difference is significant because Cirlex allows plasma discharges at higher voltages than Kapton without marked degradation of the dielectric material, thus widening the operation range of the actuator. At 11 kVpp, the maximum voltage supported by Kapton DBD, the power consumption for Kapton is ≈21 W, almost 3 times higher than the ≈8 W registered for Cirlex at the same voltage. It should be also noted that for the voltages of 12 and 13 kVpp, the Cirlex based DBDs consume less power than Kapton at 11 kVpp. In short, the Cirlex actuator consumes less power in the voltage range at which the plasma discharge is more intense and presents higher operation limit (14 kVpp), which is closely related to the compact structure of Cirlex in contrast to the multilayer structure of Kapton. In fact, although the stacking is efficient,

it does not allow to obtain a structure as homogeneous as that of Cirlex, as it is inevitable the appearance of small defects in the interface between the layers that will be reflected in the final performance of the actuator. Comparing to other materials described in the literature, the power consumption of Cirlex (≈8 W at 11 kVpp) is lower than that of polystyrene 1 mm (8.1 W at 10 kVpp), polyvinylidene fluoride 1 mm (12.8 W at 8 kVpp) and polylactic acid 1 mm (12.1 W at 10 kVpp), but higher than that of acetoxy silicone 1 mm (6.4 W at 11 kVpp) and polyisobutylene rubber 1 mm (6.3 W at 11 kVpp).[19,38] The increase of the consumed power with increasing voltage is directly related with the dielectric heating during plasma discharge, as it will be shown in Fig. 12, suggesting that most of the consumed power is dissipated by heating through the dielectric layer and only a small part is actually used to produce the airflow.[17,39] The power consumed by the DBD actuator is divided into the power delivered to the surface plasma discharge, available to induce flow velocities, and the dielectric losses of the insulating layer.[39] As the power losses in the dielectric are directly proportional to the frequency and the square of the voltage, the increase in the consumed power results from the fact that the discharge becomes unstable and markedly filamentary (detailed in Fig. 11) when voltage and frequency increase above certain threshold.[40] These results show the dependence of the power consumed by the actuators with the materials that constitute the dielectric layer, in line with previous results.[20,37] Cirlex polyimide maintains its properties in extreme operating conditions[26] what makes it a high performance material.

Fig. 5 shows the Lissajous curves obtained by the current charge method through equation (2), for the voltage levels at which induced flow velocity was registered for both actuators (Fig. 8). Lissajous figures are obtained through the plot of the charge that flows into the circuit as a function of the applied voltage between electrodes.[41] For low applied electric fields, the plot of charge versus voltage is a straight line since the system behaves like a purely capacitive cell in which the charge varies proportionally to the applied voltage. In turn, when the input voltage is enough to ignite the plasma discharge, the Lissajous plot forms a typical convex figure.[42]

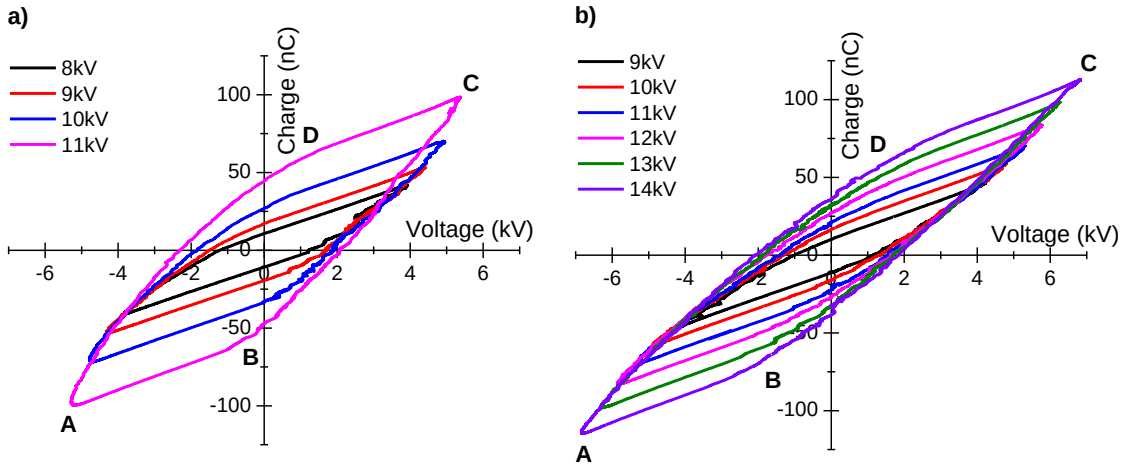


Fig. 5. Lissajous curves for Kapton (a) and Cirlex (b) DBD plasma actuators through one period of the applied voltage at 24 kHz.

The Lissajous curves presented in Fig. 5 are anticlockwise with respect to time, and each half cycle represents two branches corresponding to the moments of the plasma discharge on (BC and DA) and off (AB and CD). It can be observed that for both DBD the Lissajous figures are shaped like an ellipse featuring the so-called almond-shape cyclograms,[29] typical of the AC surface discharges,[42] instead of the parallelogram-shape Lissajous figures commonly found in volume DBD discharges.[43] This shape is a consequence of the continuous changes in the geometrical shape of the plasma discharge during the cycle, thus implying variations in the discharge capacitance.[44] The Cirlex cyclograms shapes are close to an ideal parallelogram, suitable to obtain the capacitances of the dielectric layer and plasma discharges through the respective branch slopes, whereas the Kapton curves are getting closer to an ellipse, which indicates the presence of residual ions.[45] The Cirlex Lissajous curves show sharper corners than the Kapton curves, indicating that the plasma discharge stops more abruptly for Cirlex actuators when the maximum voltage is reached,[33] which can contribute to uniform the plasma discharge. The area of the plots increases with increasing applied voltage, and is proportional to the power consumed by the DBD per cycle at each voltage level.[33] The variation of the area with input voltage agrees with the electric consumed power shown in Fig. 4. From the analysis of the cyclograms, it is noticeable that the increase of the consumed power with voltage increasing is more uniform for Cirlex than Kapton. The increments between each voltage

level are regular for the Cirlex DBD, which indicates a more uniform and homogeneous plasma discharge for this material.

Fig. 6 shows a comparison of the Lissajous curves of Kapton and Cirlex DBD actuators for 11 kVpp input voltage and 24 kHz of frequency.

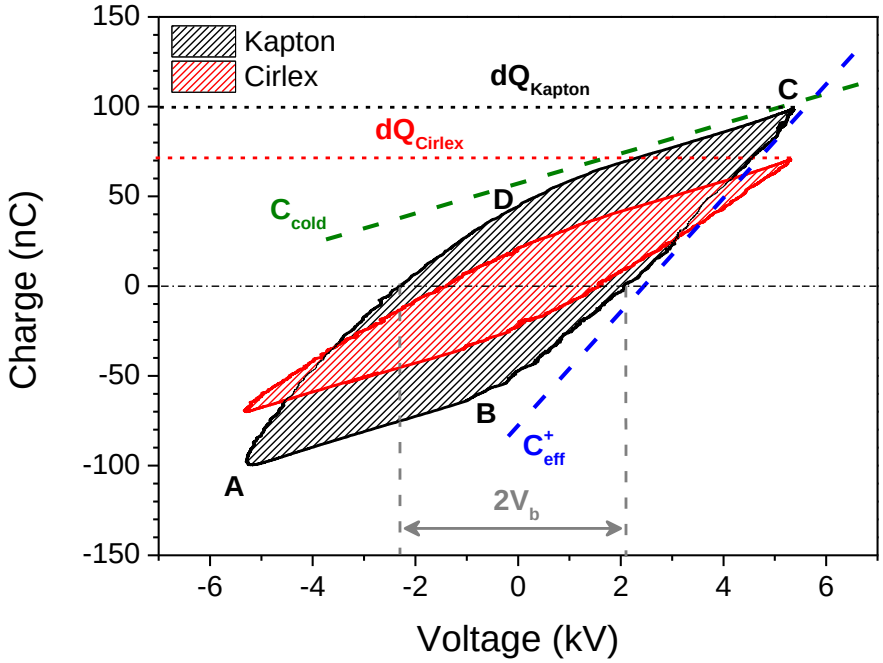


Fig. 6. Comparison between Lissajous curves for Kapton and Cirlex DBD for 11 kVpp at 24 kHz.

Fig. 6 shows that the results obtained for the consumed power by the electric current method (Fig. 4) agree with the results registered for the electric charge method. The area of the plot for the Kapton DBD is significantly larger than that for Cirlex at 11 kVpp, which is the maximum operation voltage supported by the Kapton actuator. As expected, the total charge transferred (dQ) to the Kapton DBD actuator during the AC voltage cycle is higher than for Cirlex, about 100 nC for Kapton vs. about 70 nC for Cirlex. The breakdown voltage (V_b), that determines the onset ignition of the plasma discharge, is higher for Kapton (≈2.2 kVpp) than for Cirlex (≈1.5 kVpp). In short, the Cirlex DBD actuator requires less energy to operate at 11 kVpp and generates similar induced velocity as will be seen below.

Fig. 7 shows the cold (C_{cold}) and effective (C_{eff}) capacitances extracted from the Lissajous curves of both actuators through the slopes of each branch of the positive (ABC) and negative (CDA) half cycles, as depicted in Fig. 6. The discharge of the DBD actuator is

intermittent and during each cycle there are two discharge periods (BC and DA) and two dark zones (AB and CD).[33] C_{cold} is ascribed to the pure passive component capacitance of the DBD, representing the capacitance when there is no charge transfer and the plasma is off. C_{eff} results from the combination of the passive component and the contribution of the plasma discharge, thus representing the capacitance of the DBD when the plasma discharge is occurring.[27,43]

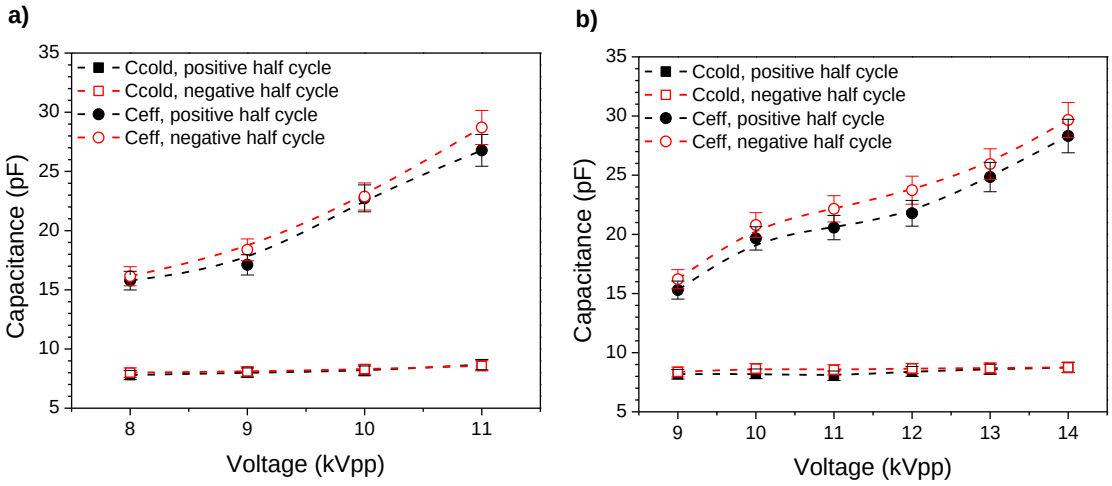


Fig. 7. Cold and effective capacitances calculated for the positive and negative half cycles from the Lissajous curves for both DBD actuators: a) Kapton and b) Cirlex.

Fig. 7 shows that the capacitances of both DBD present similar trend throughout the measured voltage range. C_{cold} remains, as expected, approximately constant independently of the applied voltage, since it depends on the passive component of the plasma actuator. The average C_{cold} for Kapton DBD is 8.2 pF, which is slightly lower than that reported in some recent literature (12.01 pF[32] and 11.81 pF[31]), and for Cirlex is 8.5 pF. In turn, C_{eff} increases with increasing applied voltage for both actuators. For Kapton DBD C_{eff} increases from ≈16 to 28 pF for 8 and 11 kVpp input voltage, similar to the values found in the literature for the same material (15.46 to 21.30 pF for 8 and 11 kVpp[31]), whereas for Cirlex actuator C_{eff} varies between ≈16 and 30 pF for the wider applied voltage range of 9 to 14 kVpp. The increase of C_{eff} with increasing applied voltage for both actuators can be related with the extension of the plasma discharge region to positions far from the exposed electrode for higher voltages,[42] as can be observed in Fig. 11 for the Cirlex actuator. It is noteworthy that the C_{eff} of the negative half cycle is relatively higher than that of the positive half cycle for both DBD actuators, which is found to be associated with the fact that during the negative half cycle the electrons

accumulate on the insulating surface, contrary to the positive half cycle wherein the electrons move from the insulating layer towards the exposed electrode leaving the discharge gap.[42] Nevertheless, these differences on C_{eff} between the positive and the negative half cycles are of minor importance since the values only differ slightly, their quotient being ≈1.[29] In short, these results agree with previous ones, showing that less charge per cycle is transferred to the Cirlex actuator than to that of Kapton at the same applied voltage, and even for the highest voltage level of 14 kVpp the charge transferred to the Cirlex actuator (≈ 30 pF) is similar to that of Kapton for 11 kVpp (≈29 pF). An accurate knowledge of these electrical parameters of the plasma discharge is essential for an adequate impedance matching or suitable design of the system control-circuit for the application of the devices in active flow control.[29]

Fig. 8 shows the maximum induced flow velocity as a function of the applied voltage obtained by Pitot tube measurements at 1.5 mm from the surface of the actuator.

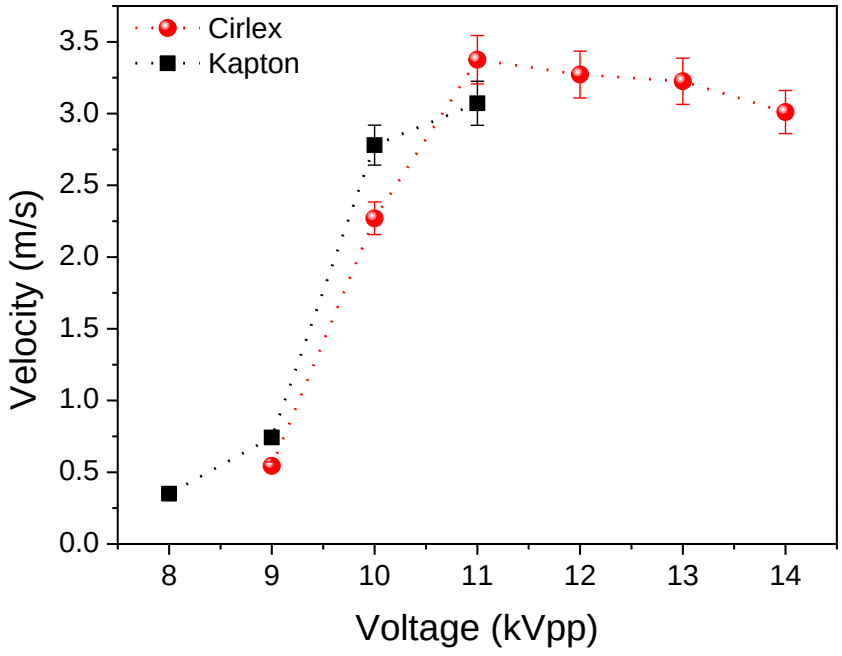


Fig. 8. Maximum induced flow velocity for Cirlex and Kapton DBD plasma actuators as a function of applied voltage at 24 kHz.

The Kapton actuator leads to induced flow velocities from 8 up to 11 kVpp, its maximum operating voltage (Fig. 3), while DBD Cirlex actuator induces flow velocities between 9 and 14 kVpp. Further, both actuators record the maximum velocity for the applied voltage of 11 kVpp, ≈3.1 m/s for Kapton and ≈3.4 m/s for Cirlex, in the same range of that found

for Kapton actuators at the same input voltage (≈3.4 m/s at 11 kVpp).[19] For these voltage ranges, and comparing with related DBD systems in the literature in studies performed under similar experimental conditions, the flow velocity recorded for Cirlex (≈3.4 m/s) is higher than that reported for polystyrene 1 mm (≈2.9 m/s at 10 kVpp), polylactic acid 1 mm (≈2.9 m/s at 10 kVpp) and silicone 1 mm (≈3.0 m/s at 11 kVpp), being lower than for polyisobutylene rubber 1 mm ((≈3.9 at 11 kVpp).[19,38]

For lower voltage levels, between 9 to 10 kVpp, the Kapton actuator induces higher velocity than Cirlex (≈2.8 m/s for 10 kVpp), while for 11 kVpp applied voltage, the Cirlex actuator induces higher velocity than Kapton. For voltages levels higher than 11 kVpp only the Cirlex DBD records induced velocities, the values slightly decreasing, although it can be considered that the flow velocity stabilizes in the plateau of around 3 m/s. In general, it is observed that the maximum induced velocity of Cirlex DBD is higher than that of Kapton, the Cirlex actuator inducing velocities around 3 m/s beyond the Kapton operating limit up to at least 14 kVpp, thus allowing its use in higher voltage ranges maintaining the flow velocity levels.

To analyse the behaviour of the induced flow for a given input voltage, the velocity profiles were plotted and the data fitted with a skewed Gaussian curve described by the equation (4):[46]

$$V_{fit} = a.\sqrt{Y}\, exp\left[-(\frac{y-b}{c})^2\right] \qquad (4)$$

where a, b and c are adjustable parameters. The analytical fit is required to obey the no-slip condition. Fig. 9 shows two representative velocity profiles of both DBD plasma actuators at 11 kVpp, the input voltage at which the highest induced velocities were recorded.

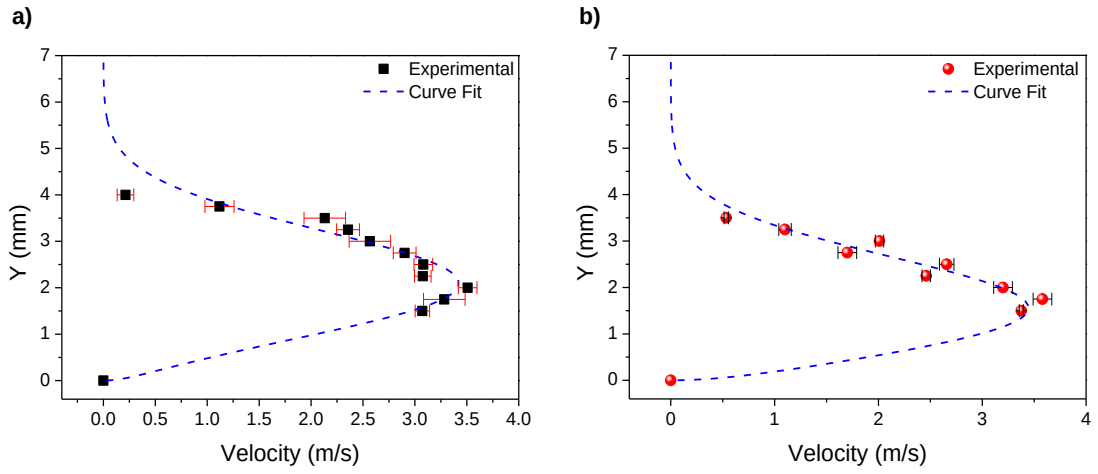


Fig. 9. a) Velocity profiles of the flow induced by the DBD plasma actuators of a) Kapton and b) Cirlex.

The velocity profiles of both actuators present the typical shape of a wall-jet flow. The velocity initially increases slightly with increasing height, up to a maximum of 2 mm, and then progressively decreases tending infinitely towards zero. The behaviour is similar for both materials, observing a good fit between the experimental behaviour and the theoretical model. For Cirlex, the decrease of the velocity is gradual with increasing height, whereas in the case of Kapton it occurs more abruptly, which may be related with the lower operation voltage limit for this material. The maximum velocity is slightly higher for Cirlex, in agreement with the results shown in Fig. 8.

Fig. 10 represents the mechanical power (P_m) and the electromechanical efficiency (η_m) as a function of the applied voltage for both actuators determined by equations (3) and (4), respectively. The mechanical power quantification is useful to evaluate the performance of the DBD actuators, since it describes the power delivered by the actuator to generate the induced flow, considering that it corresponds to the balance of kinetic energy density flow rate, under the assumption of a stationary flow. The correlation between the mechanical power and the consumed electrical power allows estimating the electromechanical efficiency of the DBD plasma actuator.[40]

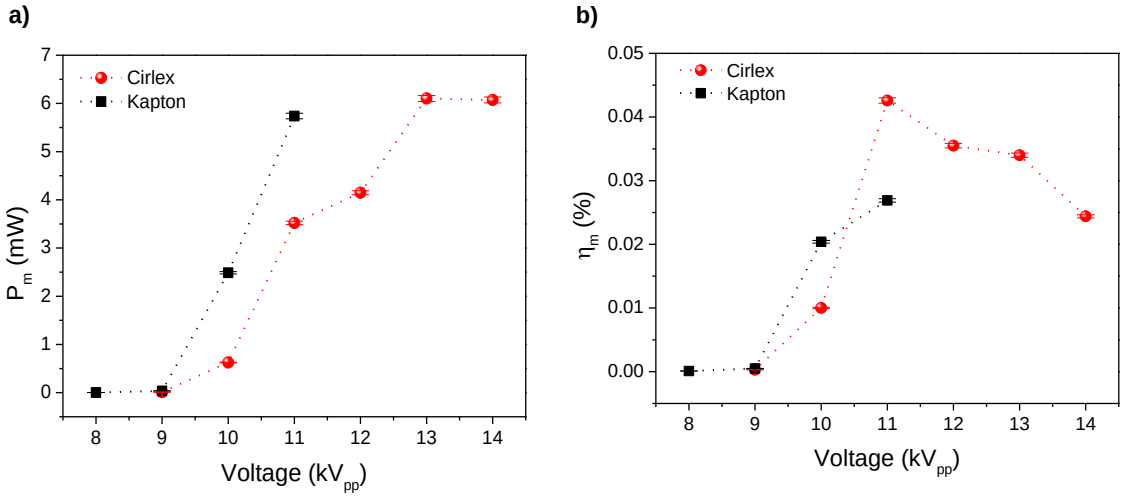


Fig. 10. a) Mechanical power and b) electromechanical efficiency of Cirlex and Kapton DBD plasma actuators for the different operation voltages at 24 kHz.

The mechanical power delivered to induce the flow velocity is in the order of miliWatts, which is low compared to the electrical power consumed by the actuators to ignite the

plasma discharge. The mechanical power added to the airflow by the plasma discharge increases with increasing applied voltage for both actuators (Fig. 10a), the Kapton DBD reaching a maximum value of around 5.7 mW at 11 kVpp, while the Cirlex actuator registers a maximum mechanical power of ≈6.1 mW for the applied voltages of 13 and 14 kVpp. These values are consistent with those found in the literature for DBD actuators with similar geometrical configuration (Kapton, 4.75 mW for 12 kVpp).[19]

Regarding the electromechanical efficiency (Fig. 10b), for the Kapton actuator it increases with increasing applied voltage registering the maximum of ≈0.03% at 11 kVpp. For the Cirlex DBD the electromechanical efficiency increases with applied voltage up to 11 kVpp, then decreasing to higher voltages between 12 and 14 kVpp. The maximum efficiency for Cirlex is ≈0.04%, recorded for the same voltage as the maximum Kapton efficiency, 11 kVpp. The mechanical efficiency of both actuators is relatively low, however these values agree with that found in the literature for similar DBD actuator systems (Kapton 0.023% for 12 kVpp).[19,27] Despite the low electromechanical efficiency of the DBD plasma actuators, they can be highly effective in flow control applications since it relies on their ability to introduce small perturbations in the flow.[40]

The analysis of the plasma discharge visualisation is useful and allows inferring several properties of the discharge and its implications on the performance of the DBD actuator. Fig. 11 allows to visualise of the surface plasma discharge in air for the Cirlex DBD actuator at different applied voltages.

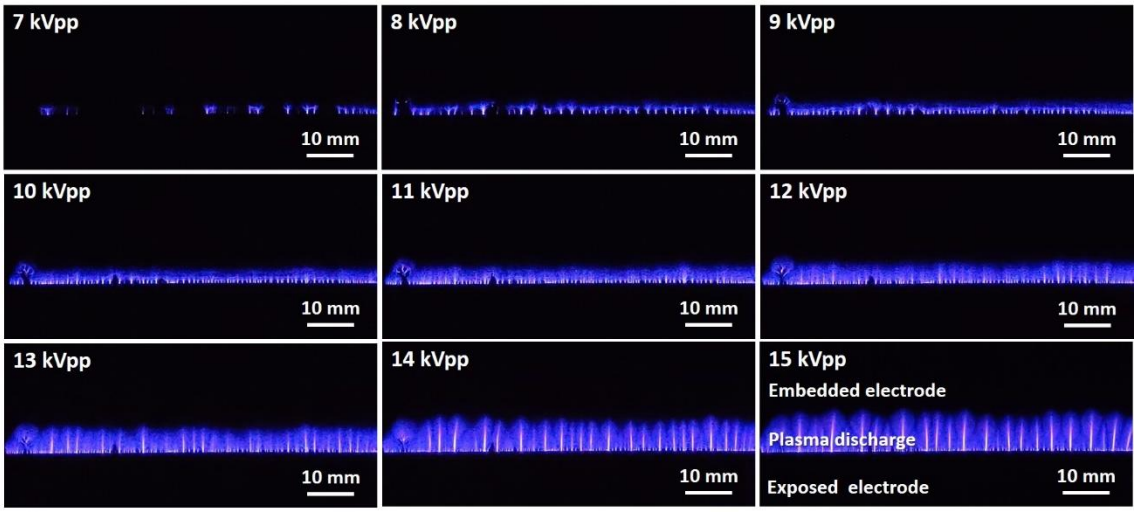


Fig. 11. Plasma visualization of Cirlex DBD actuator for different applied voltage levels at 24 kHz.

Fig. 11 allows to verify that the plasma discharge for the Cirlex DBD actuator presents the typical blue colour[47] of the ionized air. The luminosity of the surface plasma increases with increasing applied voltage, as well as the length of the plasma discharge that reaches the maximum of ≈8 mm for 15 kVpp, measured in the direction perpendicular to the edge of the exposed electrode. The increase of the applied voltage leads to a uniform discharge plasma up to 11-12 kVpp. Fig. 11 allows to observe the different regimes of the discharge during DBD operation. For the voltages of 7 and 8 kVpp the plasma discharge is non uniform being located at some certain visible points, the discharge being in the so-called spot regime, in which the induced flow velocity is negligible,[40] as shown in Fig. 8. By increasing the applied voltage to 9 kVpp, the plasma starts to become uniform forming the denominated streamer discharge, and for voltages between 10 and 12 kVpp the plasma resembles a normal glow discharge, before entering in a filamentary regime from 13 kVpp, in which the current concentrates in few filaments and the discharge is governed by the streamers, becoming difficult to control and propitiating the appearance of sparks.[40] The formation of streamers indicates saturation and that the operating limit of the actuator has been reached since, once formed, further increases in the applied voltage leads to an increase in the power dissipation without practical effects in the induced flow velocity,[16] as shown in Fig. 10b with the decrease of the mechanical efficiency from 11 kVpp, and in Fig. 8 with the induced velocity stagnation around 3 m/s from 11 kVpp. From 13 kVpp, the plasma discharge boundary line becomes irregular which is another indicator of the saturation and instability of the discharge. The complete evolution of plasma discharging with increasing input voltage can be also observed in the Video file submitted as supplementary information.

The heating of the actuator is one of the limiting factors of its operation during plasma discharge and, as mentioned earlier, a significant part of the power consumed is dissipated in the form of heat.[17] Thus, it is important to study the thermal behaviour of the dielectric layer during plasma discharge. Infrared thermography in quiescent air was conducted and the obtained thermograms as shown in Fig. 12. Since a surface with a temperature above absolute zero emits electromagnetic radiation directly proportional to its intrinsic temperature,[48] part of this radiation is infrared and can be used to determine the surface temperature. In this sense, the temperature field of the DBD actuator was obtained immediately after 180 s of operation, since it was very similar to the plasma temperature.[37] For comparing the thermal behaviour of the Kapton and Cirlex dielectric

layers, thermograms for discharge at 10 kVpp and 24 kHz are presented for both materials.

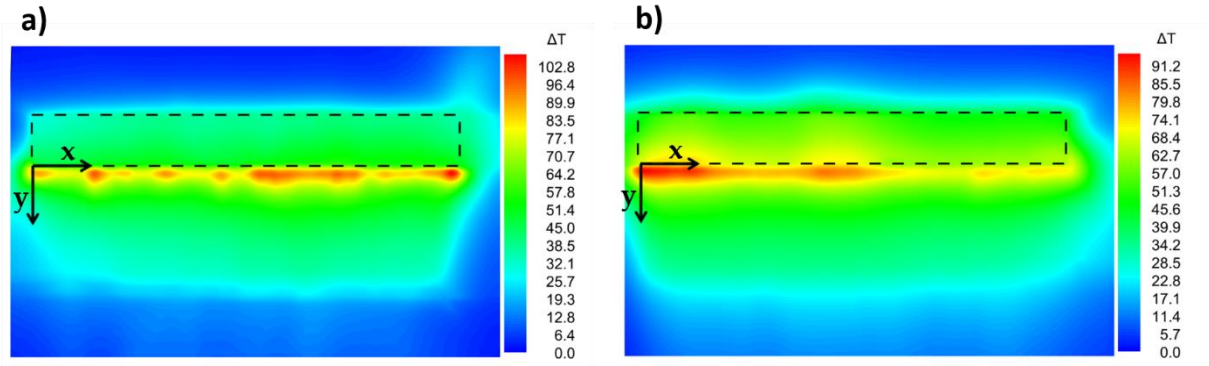


Fig. 12. Thermograms of Kapton (a) and Cirlex (b) for 10 kVpp at 24 kHz.

In Fig. 12 the asymmetry of the DBD actuator's electrodes is along the positive direction of the y axis and the dashed square corresponds to the exposed electrode. Comparing the temperature field of both DBD, lower temperature differences are registered for the Cirlex actuator (Fig. 12b) with temperature variations up to about 90 ºC whereas the Kapton actuator (Fig. 12a) reaches variations above 100 ºC. It is thus verified a direct relationship between the power consumption (Fig. 4) and the temperature, the Kapton DBD consuming more power than Cirlex at 10 kVpp and presenting a thermogram with higher temperatures, which also results in a greater energy dissipation in the form of heat. The maximum temperatures are located near the edge of the exposed electrode for both DBD, in the area where the plasma discharge occurs. In the Kapton thermogram it is possible to observe several asymmetries near to the edge of the exposed electrode along the x axis (spanwise direction), indicating a filamentary plasma discharge with localized hot spots, typical of a plasma discharge close to the limit of the dielectric material.[23] The Cirlex thermogram presents a more uniform distribution of the temperature, not only along the edge of the exposed electrode, but also in the entire thermogram. Next to the origin of the xy coordinate (left side of the thermogram) it is visible an area with a higher temperature concentration, which extends along the exposed electrode edge in the direction of the x axis, which is due to the proximity of the connection between the electrode and the high voltage cable. The temperature of Cirlex actuator is higher than Kapton in the zone of the exposed electrode and in the area where the plasma discharge spreads along the dielectric layer in the direction of y axis (streamwise direction), the zone correspondent to the embedded electrode. The higher uniformity of the temperatures for the Cirlex DBD

indicates a more stable operation at 10 kVpp, further away from its operating limit, and as expected a higher resistance than Kapton to the increasing of temperature, not affecting its performance. Despite the dielectric constant, dielectric strength and thermal conductivity of Kapton and Cirlex are very similar, the dissipation factor of Cirlex (0.0040) being higher than that of Kapton (0.0020),[15,26] which can be relevant in the performance of both materials as dielectric layers in DBD plasma actuators. The regularity of the dielectric surface has already been reported as an important factor influencing the temperature distribution of the plasma discharge,[20] and the Cirlex surface is more uniform and regular than that of Kapton, in addition to its compact structure that contrasts with the Kapton multilayer. Moreover, the thermal properties observed for Cirlex dielectric are a promising indicator for the recent trends of DBD plasma actuators applications in deicing and anti-icing systems.[49,50]

The temperature variations were analyzed along the x axis in the adjacent points of the exposed electrode's edge from x/l = -0.05 to 1.05, and along the y axis from the middle point of the exposed electrode between y/w = 0 and 3.2, where l and w are the length and the width of the exposed electrode, respectively. The results are shown in Fig. 13 for both DBD actuators at the input voltages of 8 to 10 kVpp at 24 kHz.

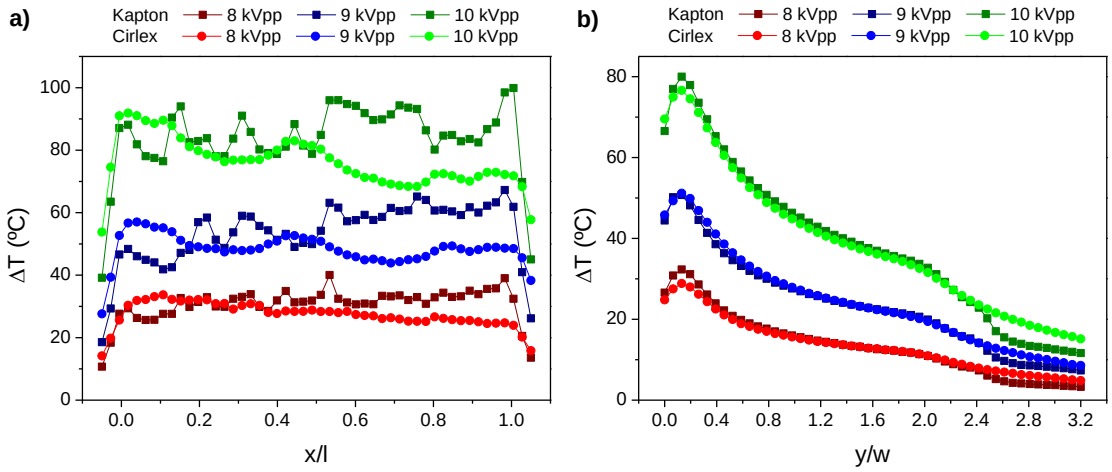


Fig. 13. Spatial temperature variation along the x axis (a) and y axis (b) for Kapton and Cirlex actuators at different input voltages.

Fig. 13 shows a clear tendency for the temperature to increase with increasing input voltage, in both directions, for the two dielectric materials. The temperature distribution along the x axis (Fig. 13a) is more uniform for Cirlex than for Kapton, and with increasing input voltage the temperature distribution becomes asymmetric for both materials. For Cirlex actuator at 8 kVpp, the curve of temperature is almost linear between x/l = 0.0 to

1.0, the area corresponding to the total length of the electrode, with a downward trend of ≈6 ºC from left to right due to the distance from the high voltage connection. For 9 kVpp, some fluctuations are observed in the curve that could be ascribed to a non-uniform plasma discharge according to the streamer mode observed in Fig. 11, which originates localized increases in the temperature along the discharge. Anyway, the tendency to temperature decrease along the x axis remains between l/x = 0.0 and 1.0 from ≈57 to 49 ºC, respectively. For 10 kVpp the curve has an identical shape of the previous one, with similar fluctuations in the same zones, but for higher temperature variations between ≈92 and 72 ºC for l/x = 0.0 and 1.0, respectively. The Kapton actuator presents irregular temperature profiles for all applied voltages and these irregularities are accentuated with increasing of input voltage signal. The lower voltage operating limit of Kapton dielectric may be in the origin of these irregular profiles, once at these voltage levels the plasma discharge enters in a filamentary regime providing non-uniform discharges, as already reported for Kapton based DBD actuators.[37] The temperature profiles along the y axis (Fig. 13b) are very similar for both dielectric materials, presenting identical shape and the same trend for all applied voltages. The maximum temperature is registered near to the exposed electrode edge for y/w = 0 in the zone that the plasma discharge onsets, so the temperature of the dielectric is slightly higher than that of the electrode. Next, the temperature decays sharply up to y/w ≈ 0.5 and smoothly until y/w ≈ 2, which corresponds approximately to the end of the embedded electrode and the limit of the plasma discharge extension. For Kapton actuators, a further decay is observed in the temperature around y/w ≈ 2.5, corresponding to the end of the dielectric layer itself.

Conclusions

DBD plasma actuators based on Cirlex and Kapton polyimides were assembled and their electrical, dielectrical, mechanical, electromechanical and thermal properties were assessed in view of active flow control applications. The Cirlex DBD presents lower power consumption than Kapton and higher voltage operation limit of at least 14 kVpp. The charge transferred during the AC cycle at 11 kVpp for Cirlex (70 nC) is lower than Kapton (100 nC), as well as the dielectric breakdown of 1.5 kVpp against 2.2 kVpp, respectively. The cold capacitance is lower for Kapton (8.2 pF against 8.5 pF) whereas the effective capacitance is lower for Cirlex in the entire measured voltage range: ≈16 to 30 pF for 9 to 14 kVpp (Cirlex) compared to ≈16 to 28 pF for 8 to 11 kVpp (Kapton).

The Cirlex DBD induced higher maximum flow velocity of ≈3.4 m/s compared to ≈3.1 m/s for Kapton at 11 kVpp. The mechanical power delivered by the Cirlex actuator is 6.2 mW with an electromechanical efficiency of 0.04%, whereas for Kapton is 5.8 mW and 0.03%, both at 11 kVpp. The plasma discharge for Cirlex actuator is stable and uniform from 10 to 12 kVpp. The temperature fields and thermal profiles of Cirlex DBD are more uniform and regular than that of Kapton, and Kapton dissipates more energy in form of heat. It can be concluded that the use of a polyimide of unique and compact structure (Cirlex) is advantageous over stacking micrometric layers (Kapton) for the development of DBD plasma actuators. Cirlex polyimide represents therefore a suitable alternative to Kapton polyimide, the corresponding DBD plasma actuators consuming and dissipating less energy, having higher voltage operation limit, generating higher induced flow velocity, delivering higher mechanical power, presenting higher electromechanical efficiency, and demonstrating itself as a more robust and durable device. This set of improvements will allow to optimize the performance of a DBD plasma actuators, improving efficiency in the production of ionic wind, which makes them more environmentally friendly.

Acknowledgements

The authors thank the Fundação para a Ciência e a Tecnologia (FCT), Fundo Social Europeu (FSE) and Programa Operacional Regional Centro 2020 and Norte 2020 for the Strategic Funding UID/00151/2020 and UID/FIS/04650/2020, the grant SFRH/BPD/117838/2016 (J.N.P.) and the project CEECIND/03347/2017 (M.A.). F.F.R. wish to thank the financial support of the project INDTECH 4.0 funded by Portugal 2020, Programa Operacional Competitividade e Internacionalização (POCI) and Fundo Europeu de Desenvolvimento Regional (FEDER). The authors acknowledge funding from the Basque Government Industry Departments under the ELKARTEK programs.

References

1. Wang J, Feng L. Introduction. In: Shyy W, Yang V, eds. *Flow control techniques and applications*. Cambridge University Press; 2019:1-19. *Cambridge Aerospace Series*.

2. Neretti G. Active flow control by using plasma actuators. In: Agarwal RK, ed. *Recent progress in some aircraft technologies*. IntechOpen; 2016:57-76.

3. Opaits DF. *Dielectric barrier discharge plasma actuator for flow control*. 2012:1-162. NASA/CR—2012-217655. https://ntrs.nasa.gov/search?reportNumber=NASA%2FCR-2012-217655

4. DiChen, KengoAsada, SatoshiSekimoto, KozoFujii, HiroyukiNishida. A high-fidelity body-force modeling approach for plasma-based flow control simulations. *Physics of Fluids*. 2021;33(3):037115. doi:https://doi.org/10.1063/5.0040987

5. Abdollahzadeh M, Pascoa JC, Oliveira PJ. Comparison of DBD plasma actuators flow control authority in different modes of actuation. *Aerospace Science and Technology*. 2018/07/01/ 2018;78:183-196. doi:https://doi.org/10.1016/j.ast.2018.04.013

6. Karimi S, Mohammadikalakoo B, Schito P. Performance enhancement of single dielectric barrier discharge flow control actuators by means of rear linking tunnels on a reference bluff body using CFD. *Journal of Wind Engineering and Industrial Aerodynamics*. 2021/02/01/ 2021;209:104488. doi:https://doi.org/10.1016/j.jweia.2020.104488

7. Abdelraouf H, Elmekawy AMN, Kassab SZ. Simulations of flow separation control numerically using different plasma actuator models. *Alexandria Engineering Journal*. 2020/10/01/ 2020;59(5):3881-3896. doi:https://doi.org/10.1016/j.aej.2020.06.044

8. Abdollahzadeh M, Pascoa JC, Oliveira PJ. Implementation of the classical plasma–fluid model for simulation of dielectric barrier discharge (DBD) actuators in OpenFOAM. *Computers & Fluids*. 2016/04/10/ 2016;128:77-90. doi:https://doi.org/10.1016/j.compfluid.2016.01.012

9. Abdollahzadeh M, Rodrigues F, Pascoa JC, Oliveira PJ. Numerical design and analysis of a multi-DBD actuator configuration for the experimental testing of ACHEON nozzle model. *Aerospace Science and Technology*. 2015/02/01/ 2015;41:259-273. doi:https://doi.org/10.1016/j.ast.2014.12.012

10. Mahdavi H, Daliri A, Sohbatzadeh F, Shirzadi M, Rezanejad M. A single unsteady DBD plasma actuator excited by applying two high voltages simultaneously for flow control. *Physics of Plasmas*. 2020;27(8):083514. doi:https://doi.org/10.1063/5.0010069

11. Yoneda H, Goto A, Kato H, Sekimoto S, Fujii K. Flight test of UAV with DBD-Pa flow control. presented at: AIAA Scitech 2021 Forum; 2021; Virtual Event. Session Flow Control for Flight. https://doi.org/10.2514/6.2021-1942

12. Baranov SA, Chernyshev SL, Khomich VY, et al. Experimental cross-flow control in a 3D boundary layer by multi-discharge plasma actuators. *Aerospace Science and Technology*. 2021/05/01/ 2021;112:106643. doi:https://doi.org/10.1016/j.ast.2021.106643

13. Harinaldi, Kesuma MD, Irwansyah R, Julian J, Satyadharma A. Flow control with multi-DBD plasma actuator on a delta wing. Article. *Evergreen*. 2020;7(4):602-608. doi: http://dx.doi.org/10.5109/4150513

14. Shadmani S, Mojtaba M, Mojtaba Mousavi Nainiyan S, Mirzaei M, Ghasemiasl R, Pouryoussefi S. Experimental investigation of flow control over an Ahmed body using DBD plasma actuator. *J Appl Fluid Mech*. 2018;11:1267-1276. doi:https://doi.org/10.18869/acadpub.jafm.73.248.28600

15. DuPont. Kapton® Polyimide films - Kapton® HN. DuPont. Accessed July, 2021, https://www.dupont.com/products/kapton-hn.html

16. Thomas FO, Corke TC, Iqbal M, Kozlov A, Schatzman D. Optimization of dielectric barrier discharge plasma actuators for active aerodynamic flow control. *AIAA Journal*. 2009;47(9):2169-2178. doi:https://doi.org/10.2514/1.41588

17. Pons J, Moreau E, Touchard G. Asymmetric surface dielectric barrier discharge in air at atmospheric pressure: electrical properties and induced airflow characteristics. *Journal of Physics D: Applied Physics*. 2005/09/16 2005;38(19):3635-3642. doi:https://doi.org/10.1088/0022-3727/38/19/012

18. Cattafesta III LN, Sheplak M. Actuators for active flow control. *Annual Review of Fluid Mechanics*. 2011;43(1):247-272. doi:https://doi.org/10.1146/annurev-fluid-122109-160634

19. Rodrigues FF, Pascoa JC, Trancossi M. Experimental analysis of alternative dielectric materials for DBD plasma actuators. presented at: ASME 2018 International Mechanical Engineering Congress and Exposition; 2018; Pittsburgh, PA, USA. Accessed 3/12/2021. https://doi.org/10.1115/IMECE2018-87455 V001T03A005

20. Rodrigues FF, Pascoa JC, Trancossi M. Experimental thermal characterization of DBD plasma actuators. presented at: ASME 2017 International Mechanical Engineering Congress and Exposition; 2017; Tampa, Florida, USA. Accessed 3/26/2021. https://doi.org/10.1115/imece2017-70541 V001T03A004

21. Wojewodka MM, White C, Kontis K. Effect of permittivity and frequency on induced velocity in ac-DBD surface and channel plasma actuators. *Sensors and Actuators A: Physical*. 2020/03/01/ 2020;303:111831. doi:https://doi.org/10.1016/j.sna.2020.111831

22. Portugal S, Roy S, Lin J. Functional relationship between material property, applied frequency and ozone generation for surface dielectric barrier discharges in atmospheric air. *Scientific Reports*. 2017/07/25 2017;7(1):6388. doi:https://doi.org/10.1038/s41598-017-06038-w

23. Ferry J, Rovey J. Thrust measurement of dielectric barrier discharge plasma actuators and power requirements for aerodynamic control. presented at: 5th Flow Control Conference; 2012; Chicago, Illinois, USA. Session FC-19: Plasma Actuators. https://doi.org/10.2514/6.2010-4982

24. Hanson RE, Houser NM, Lavoie P. Dielectric material degradation monitoring of dielectric barrier discharge plasma actuators. *Journal of Applied Physics*. 2014;115(4):043301. doi:https://doi.org/10.1063/1.4862309

25. Pescini E, Giorgi MGD, Francioso L, Taurino A, Martucci MC, Lavoie P. Electrode material degradation monitoring for durable dielectric barrier discharge

plasma actuators manufacturing. presented at: 54th AIAA Aerospace Sciences Meeting; 2016; San Diego, California, USA. https://doi.org/10.2514/6.2016-0196

26. Fralock. DuPont™ CIRLEX® Data Sheet. Accessed July, 2021, https://www.fralock.com/medical-life-science-microfluidics/materials-technical/data-sheets/cirlex-data-sheet/

27. Rodrigues F, Mushyam A, Pascoa J, Trancossi M. A new plasma actuator configuration for improved efficiency: the stair-shaped dielectric barrier discharge actuator. *Journal of Physics D: Applied Physics*. 2019/07/15 2019;52(38):385201. doi:https://doi.org/10.1088/1361-6463/ab2584

28. Kotsonis M. Diagnostics for characterisation of plasma actuators. *Measurement Science and Technology*. 2015/08/13 2015;26(9):092001. doi:https://doi.org/10.1088/0957-0233/26/9/092001

29. Kriegseis J, Möller B, Grundmann S, Tropea C. Capacitance and power consumption quantification of dielectric barrier discharge (DBD) plasma actuators. *Journal of Electrostatics*. 2011/08/01/ 2011;69(4):302-312. doi:https://doi.org/10.1016/j.elstat.2011.04.007

30. Leger L, Moreau E, Touchard G. Electrohydrodynamic airflow control along a flat plate by a DC surface corona discharge - velocity profile and wall pressure measurements. presented at: 1st Flow Control Conference; 2002; St Louis, Missouri, USA. Session FC-4: Boundary Layer Control. https://doi.org/10.2514/6.2002-2833

31. Rodrigues FF, Pascoa JC. Implementation of stair-shaped dielectric layers in micro- and macroplasma actuators for increased efficiency and lifetime. *Journal of Fluids Engineering*. 2020;142(10):104502. doi: https://doi.org/10.1115/1.4047800

32. Rodrigues F, Pascoa J, Trancossi M. Heat generation mechanisms of DBD plasma actuators. *Experimental Thermal and Fluid Science*. 2018/01/01/ 2018;90:55-65. doi:https://doi.org/10.1016/j.expthermflusci.2017.09.005

33. Manley TC. The electric characteristics of the ozonator discharge. *Transactions of The Electrochemical Society*. 1943;84(1):83. doi:https://doi.org/10.1149/1.3071556

34. Benard N, Moreau E. Role of the electric waveform supplying a dielectric barrier discharge plasma actuator. *Applied Physics Letters*. 2012;100(19):193503. doi:https://doi.org/10.1063/1.4712125

35. Benard N, Noté P, Caron M, Moreau E. Highly time-resolved investigation of the electric wind caused by surface DBD at various ac frequencies. *Journal of Electrostatics*. 2017/08/01/ 2017;88:41-48. doi:https://doi.org/10.1016/j.elstat.2017.01.018

36. Debien A, Benard N, Moreau E. Streamer inhibition for improving force and electric wind produced by DBD actuators. *Journal of Physics D: Applied Physics*. 2012/05/10 2012;45(21):215201. doi:https://doi.org/10.1088/0022-3727/45/21/215201

37. Rodrigues FF, Pascoa JC, Trancossi M. Experimental analysis of dielectric barrier discharge plasma actuators thermal characteristics under external flow influence. *Journal of Heat Transfer*. 2018;140(10)doi:https://doi.org/10.1115/1.4040152

38. F. F. Rodrigues, J. Nunes-Pereira, M. Abdollahzadeh, J. Pascoa, Lanceros-Mendez S. Comparative evaluation of dielectric materials for plasma actuators active flow control and heat transfer applications. presented at: Proceedings of the ASME 2021, Fluids Engineering Division Summer Meeting, FEDSM2021; August 10-12, 2021 2021; Virtual, Online. https://doi.org/10.1115/FEDSM2021-65748

39. Roth JR, Dai X, Rahel J, Sherman D. The physics and phenomenology of paraelectric one atmosphere uniform glow discharge plasma (OAUGDP) actuators for aerodynamic flow control. presented at: 43rd AIAA Aerospace Sciences Meeting and Exhibit; 10-13 January 2005 2005; Reno, Nevada, USA. Session WIG-4: Plasma Aerodynamics II. https://doi.org/10.2514/6.2005-781

40. Moreau E. Airflow control by non-thermal plasma actuators. *Journal of Physics D: Applied Physics*. 2007/01/19 2007;40(3):605-636. doi:https://doi.org/10.1088/0022-3727/40/3/S01

41. Falkenstein Z, Coogan JJ. Microdischarge behaviour in the silent discharge of nitrogen - oxygen and water - air mixtures. *Journal of Physics D: Applied Physics*. 1997/03/07 1997;30(5):817-825. doi:https://doi.org/10.1088/0022-3727/30/5/015

42. Biganzoli I, Barni R, Gurioli A, Pertile R, Riccardi C. Experimental investigation of Lissajous figure shapes in planar and surface dielectric barrier discharges. *Journal of Physics: Conference Series*. 2014/11/26 2014;550:012039. doi:https://doi.org/10.1088/1742-6596/550/1/012039

43. Jiang H, Shao T, Zhang C, et al. Experimental study of Q-V Lissajous figures in nanosecond-pulse surface discharges. *IEEE Transactions on Dielectrics and Electrical Insulation*. 2013;20(4):1101-1111. doi:https://doi.org/10.1109/TDEI.2013.6571423

44. Gibalov VI, Pietsch GJ. The development of dielectric barrier discharges in gas gaps and on surfaces. *Journal of Physics D: Applied Physics*. 2000/09/29 2000;33(20):2618-2636. doi:https://doi.org/10.1088/0022-3727/33/20/315

45. Kogelschatz U. Dielectric-barrier discharges: their history, discharge physics, and industrial applications. *Plasma Chemistry and Plasma Processing*. 2003/03/01 2003;23(1):1-46. doi:https://doi.org/10.1023/A:1022470901385

46. Hoskinson AR, Hershkowitz N, Ashpis DE. Force measurements of single and double barrier DBD plasma actuators in quiescent air. *Journal of Physics D: Applied Physics*. 2008/11/27 2008;41(24):245209. doi:https://doi.org/10.1088/0022-3727/41/24/245209

47. Davidson G, O'Neil R. Optical radiation from nitrogen and air at high pressure excited by energetic electrons. *The Journal of Chemical Physics*. 1964;41(12):3946-3955. doi:http://dx.doi.org/10.1063/1.1725841

48. Vollmer M, Möllmann K-P. Fundamentals of Infrared Thermal Imaging. *Infrared Thermal Imaging: Fundamentals, Research and Applications*. 2nd Edition ed. Wiley-VCH; 2018:1-106.

49. Abdollahzadeh M, Rodrigues F, Pascoa JC. Simultaneous ice detection and removal based on dielectric barrier discharge actuators. *Sensors and Actuators A: Physical*. 2020/11/01/ 2020;315:112361. doi:https://doi.org/10.1016/j.sna.2020.112361

50. Rodrigues F, Abdollahzadeh M, Pascoa J, Oliveira PJ. An experimental study on segmented-encapsulated electrode dielectric-barrier-discharge plasma actuator for mapping ice formation on a surface: a conceptual analysis. *Journal of Heat Transfer*. 2021;143(1)doi:https://doi.org/10.1115/1.4048252

Graphical Abstract

